Proceedings of the ASME 2019
Gas Turbine India Conference
GTINDIA2019
December 5-6, 2019, Chennai, Tamil Nadu, India

GTINDIA2019-2628

NUMERICAL PREDICTION OF COOLING PERFORMANCE SENSITIVITY OF 1ST STAGE NOZZLE GUIDE VANE UNDER AEROTHERMAL CONDITIONS

Prasert Prapamonthon[1,2,*], Bo Yin[1,*]
[1] Key Laboratory for Mechanics in Fluid Solid Coupling Systems, Institute of Mechanics, Chinese Academy of Sciences, Beijing, 100190, China

[2] Department of Aeronautical Engineering, International Academy of Aviation Industry, King Mongkut's Institute of Technology Ladkrabang, Bangkok 10520, Thailand

Guowei Yang[1], Mohan Zhang[1,3]
[1] Key Laboratory for Mechanics in Fluid Solid Coupling Systems, Institute of Mechanics, Chinese Academy of Sciences, Beijing, 100190, China

[3] School of Engineering Science, University of Chinese Academy of Sciences, Beijing100049, China

ABSTRACT

To obtain high power and thermal efficiency, the 1st stage nozzle guide vanes of a high-pressure turbine need to operate under serious circumstances from burned gas coming out of combustors. This leads to vane suffering from effects of high thermal load, high pressure and turbulence, including flow-separated transition. Therefore, it is necessary to improve vane cooling performance under complex flow and heat transfer phenomena caused by the integration of these effects. In fact, these effects on a high-pressure turbine vane are controlled by several factors such as turbine inlet temperature, pressure ratio, turbulence intensity and length scale, vane curvature and surface roughness. Furthermore, if the vane is cooled by film cooling, hole configuration and blowing ratio are important factors too. These factors can change the aerothermal conditions of the vane operation. The present work aims to numerically predict sensitivity of cooling performances of the 1st stage nozzle guide vane under aerodynamic and thermal variations caused by three parameters i.e. pressure ratio, coolant inlet temperature and height of vane surface roughness using Computational Fluid Dynamics (CFD) with Conjugate Heat Transfer (CHT) approach. Numerical results show that the coolant inlet temperature and the vane surface roughness parameters have significant effects on the vane temperature, thereby affecting the vane cooling performances significantly and sensitively.

Keywords: Cooling performance, Turbine vane, cooling effectiveness, Thermal sensitivity, Aerothermal condition

NOMENCLATURE

C_s	roughness constant
C_μ	constant
E	empirical constant
k	turbulent kinetic energy
K_s	physical roughness height
K_s^+	nondimensional roughness height
$P_{s,out}$	static pressure at mainstream outlet
$P_{t,in}$	total pressure at mainstream inlet
PR	pressure ratio
q_{flux}	heat flux
T	temperature
$T_{c,in}$	temperature at coolant inlet
T_{me}	volume vane temperature
T_w	wall temperature
T_∞	temperature at mainstream inlet
U	velocity
u*	velocity parameter
u_p	mean velocity of fluid at wall-adjacent cell centroid
y_p	distance from centroid of wall-adjacent cell to wall
ΔB	adaptive constant
ρ	density
ϕ	cooling effectiveness
ν	kinematic viscosity
κ	von Karman constant
τ_w	wall shear stress

* Contact author: jinfa@imech.ac.cn, prasert.pr@kmitl.ac.th, and yinbo@imech.ac.cn

INTRODUCTION

Based on the Brayton cycle, thermal efficiency is dependent on the turbine inlet temperature. Ideally, the higher the turbine inlet temperature, the better the thermal efficiency is. Regrettably, in real situations, the allowable turbine inlet temperature is limited by the durability of hot component materials, especially airfoils of the 1st stage nozzle guide vane of high-pressure gas turbines. At high temperatures, heat transfer from high thermal load causes thermal damage, thereby reducing a lifespan of the airfoils. Therefore, a turbine airfoil of gas turbines needs effective cooling systems, including ways to prolong hour service of the airfoil. Presently, turbine airfoils of a state-of-the-art gas turbine contain internal passages for coolant supplied by the compressor. The cool air is used for internal cooling and film cooling to reduce the metal temperature. For film cooling, its objective is to protect the airfoil external surface which is under a complex flow field. These cause a variation of local heat transfer coefficient and local freestream temperature on the hot gas side and lead to a variation of the airfoil surface temperature, including temperature gradients due to heat conduction within the airfoil material. As described, heat convection from film cooling, internal cooling and heat conduction within the airfoil material are intrinsically linked, thereby making the overall thermal problem complicated and difficult. On top of that, it is important to understand the phenomena of the combined mode of heat transfer and fluid flow. The accurate prediction of heat transfer and fluid flow which is an important step for airfoil lifespan assessment needs to be done reliably. So far, aerothermal prediction on turbine airfoils has been investigated experimentally and computationally for many years. Based on the numerical approach, many researchers [1-14] have shown that the simultaneous simulation using computational fluid dynamics (CFD) and conjugate heat transfer (CHT) can predict airfoil temperature obtained from problems of three modes of heat transfer with fluid flow acceptably. Apart from using the CFD/CHT approaches to evaluate the airfoil temperature, some of the researchers also investigated effects of aerothermal uncertainties in boundary conditions and material property and specification on the airfoil surface temperature and thermal distributions. For examples, Alizadeh et al. [12] studied uncertainties on parameters that affect heat transfer parameters of turbine blades such as turbine inlet temperature and pressure, rotor coolant inlet pressure and temperature, blade metal thermal conductivity, blade coating thickness. Their results indicated that the uncertainty of these parameters has significant impacts on the blade temperature. Alizadeh et al. [13] also examined the effects of the wall temperature and inlet total temperature on cooling mass flow rate of a turbine airfoil. Additionally, the influence of inlet total temperature on cooling convective efficiency was studied. Reyhani et al. [14] studied a sensitivity of blade coating thickness, coolant inlet pressure and temperature and gas turbine load variation to turbine blade temperature calculation and life estimation. They indicated that the blade lifespan rises by 9 times when the thickness of coating increases by 3 times. Besides, Haubert et al. [15] investigated the effects of design parameters on blade life prediction. Their results showed that the heat transfer parameters are the most critical factors that result in the lifespan of the blade. Kim et al. [16] evaluated the sensitivity of operating parameters on the predicted blade temperatures and stresses. Their results showed the spatially resolved sensitivity of the operating parameters on blade temperature and stress distributions. Roos [17] carried out sensitivity analyses of the trailing edge ejection slot width on cooling performance in a nozzle guide vane. His study indicated that the reduction in the slot size causes a corresponding decrease in the coolant mass flow rate, thereby increasing in the blade temperature. Williams et al. [18] conducted sensitivity of overall effectiveness to film cooling and internal cooling on the suction surface of a turbine vane. Their investigation showed that overall cooling effectiveness increases at higher momentum flux ratios obtained from adjusting the coolant flow rate. Nadali et al. [19] performed the sensitivity analysis of blowing ratio, film hole shape and effect of hole position on film cooling performance of a real vane configuration working at engine conditions. They indicated that geometry parameters like film hole shape and hole position which are related to the blowing ratio play major roles in film cooling performance. Espinosa et al. [20] evaluated the effect of cooling airflow rate reduction on the blade surface temperature distribution. Their results showed that the temperature distribution is related to the cooling effectiveness, on the coolant flow rate in the cooling passages.

Although there have been several studies of uncertainties or deviations of parameters linked to aerothermal conditions so far, the study of effects of the parameter uncertainties is still challenging, because overall thermal problems obtained from a turbine airfoil are complicated, as mentioned previously, especially if a vane is cooled by intricate cooling systems. This work aims to numerically predict effects of some uncertainties of important parameters on cooling performances of a numerously film-cooled vane of the 1st stage nozzle guide vanes i.e. 217 film holes in total. Such parameters are as follows: (1) pressure ratio, which can be used to increase the velocity of the hot gas before entering moving blades, (2) coolant inlet temperature, which is constrained from the compressor supply, and (3) physical surface roughness height, which is existed naturally during long hour service, including in the manufacturing process.

VANE CONFIGURATION

The vane used in this work is one of the 1st stage nozzle guide vanes adopted from Halila et al. [21]. It is the same model that was used in Zhang et al. [22]. The vane is film-cooled by cooling air from 13 rows of film holes which have 217 holes in total, as shown in Fig. 1. The cooling air is supplied by two cavities i.e. forward and aft cavities. Each cavity has one baffle with many impingement holes, specifically, 131 and 216 holes for forward and aft baffles, respectively, as seen in Fig. 2. It should be noted briefly that film holes of the rows R1-R2 and R13 are a fan-shaped type and rectangular slot, respectively, whereas other holes are cylindrical with radial, axial or compound direction. More details about film holes are available in Halila et al. [21].

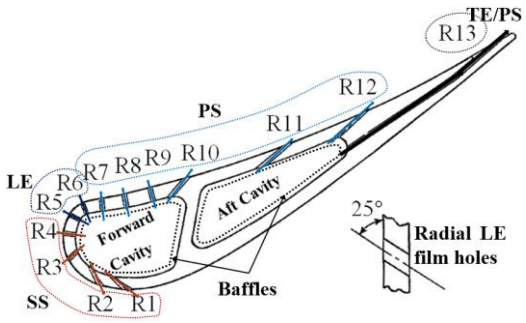

FIGURE 1: CONFIGURATION OF NOZZLE GUIDE VANE AND ITS FILM HOLES

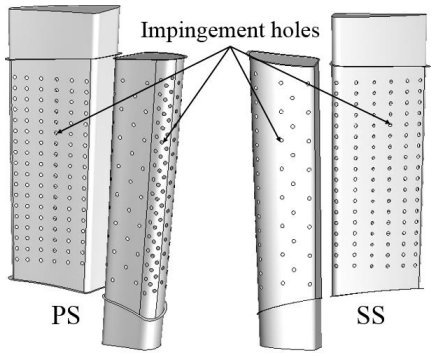

FIGURE 2: CONFIGURATION OF BAFFLES AND THEIR IMPIGEMENT HOLES

COMPUTATIONAL TECHNIQUE

The computational technique and solver setup are explained in this part. The computation mesh of the solid and fluid domains is generated by ANSYS ICEM. The mesh around the vane solid is stretched normal to the walls to obtain 8-12 layers by O-grid technique. Mesh independence was confirmed by Zhang et al. [22] through three numbers of mesh elements i.e. 7, 11 and 16 million elements. They indicated that the mesh with 11 and 16 million elements provided an insignificant difference in numerical results of the surface temperature. Thus, the 11 million element mesh is adopted for the present work and the maximum Y^+ of this mech is about 5. Fig. 3 shows the computational domain obtained by the mesh with 11 million elements and some parts of the computational mesh in the fluid and solid domains.

For the solver, ANSYS FLUENT with SST k-w model is used to compute flow filed and heat transfer using conjugate heat transfer (CHT). Based on CHT, the mesh interface technique is applied to all interfaces between the solid and fluid domains. With this technique, thermal flux can transfer across the interfaces and the surface temperatures at the interfaces of the solid and fluid domains are equivalent. Besides, the surface roughness model available in the solver is used to explore the impact of surface roughness height (K_s) on cooling performance sensitivity. By this means, the vane surface roughness is modeled as a uniform sand-grain roughness, as shown in Fig. 4. This model involves two constants i.e. roughness constant (C_s) and physical roughness height (K_s). The physical roughness height is related to the dimensionless roughness parameter as

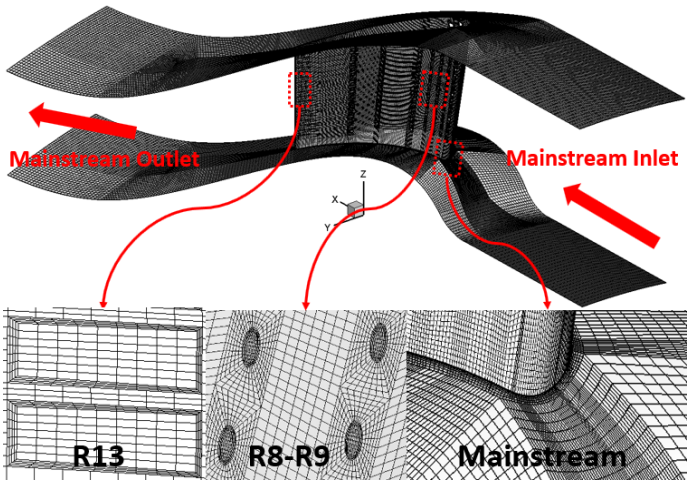

FIGURE 3: COMPUTATIONAL DOMAIN AND SOME PARTS OF COMPUTATIONAL MESH

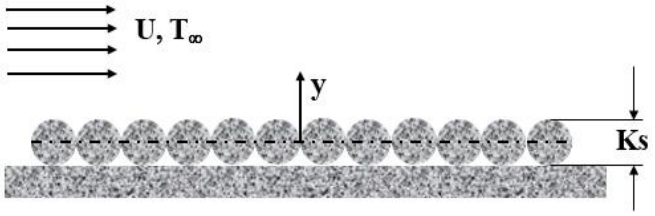

FIGURE 4: VANE SURFACE ROUGHNESS MODEL

proposed by Nikuradse [23], defining as $K_s^+ = \frac{K_s u^*}{\nu}$, where u^* is the velocity parameter which is computed from $u^* = C_\mu^{0.25} k^{0.5}$, ν denotes the kinematic viscosity, k stands for the turbulence kinetic energy, and C_μ is 0.09. The dimensionless roughness parameter is used to define the flow regime under the influence of the surface roughness. Based on the study of Nikuradse [23], the solver used in the present study divides the impact of the surface roughness on the flow field into three zones i.e. (1) hydrodynamically smooth surface ($K_s^+ \le 2.25$), (2) transitional roughness surface ($2.25 < K_s^+ \le 90$), and (3) fully rough surface ($K_s^+ > 90$). The surface roughness effect in the zone of the hydrodynamically smooth surface is ignored because it causes very low disturbances to the fully viscous sublayer in this zone. However, it becomes more and more important in the transitional roughness surface due to increasingly serious disturbances to the viscous sublayer as the dimensionless roughness parameter increases, and the viscous sublayer is destroyed completely by the full effects of the roughness in the fully rough surface zone. To study the effects of the roughness, the adaptive constant (ΔB) is evaluated as the formulas proposed by Cebeci and Bradshaw [24], as seen in the equation (1).

$$\Delta B = \begin{cases} 0 \Leftrightarrow K_s^+ \le 2.25 \\ \frac{1}{\kappa}\ln\left(\frac{K_s^+ - 2.25}{87.75} + C_s K_s^+\right) \cdot \sin[0.4258(\ln(K_s^+) - 0.811)] \\ \Leftrightarrow 2.25 < K_s^+ \le 90 \\ \frac{1}{\kappa}\ln(1 + C_s K_s^+) \Leftrightarrow K_s^+ > 90 \end{cases} \quad (1)$$

Then, ΔB is linked to calculating wall shear stress (τ_w) and mean temperature as the equation (2).

$$\frac{u_p u^*}{\tau_w/\rho} = \frac{1}{\kappa}\ln\left(E\frac{u^* y_p}{\nu}\right) - \Delta B \quad (2)$$

where u_p, y_p, E and κ are the mean velocity of the fluid at the wall-adjacent cell centroid, the distance from the centroid of the wall-adjacent cell to the wall, the empirical constant (= 9.793), and the von Karman constant (= 0.4187), respectively.

As mentioned previously, the present work is done by the CFD/CHT approach. Therefore, the convergence criteria of the numerical results are needed to define rightly. All numerical results are checked by the standard criteria of the residual of continuity ($1x10^{-3}$) and energy ($1x10^{-7}$). The convergence of the results is confirmed by monitoring the unchanged temperature with the iteration at six points on the PS, SS, LE, and TE. Furthermore, mass balance at all inlets and outlets is examined.

BOUNDARY CONDITIONS AND SIMULATION SETUP

Main boundary conditions for the hot mainstream and coolant are illustrated in Fig. 5. Most thermodynamic properties of the boundary conditions are set as experimental conditions reported by Timko [25]. For the reference case, at the mainstream inlet, temperature and total pressure are uniform with a value of 709 K and 3.402 atm, respectively. The pressure ratio (PR) defined by the ratio of the total pressure at the mainstream inlet ($P_{t,in}$) to the static pressure at the mainstream outlet ($P_{s,out}$) is used to define the boundary condition at the mainstream outlet, PR = 1.67. At the forward and aft coolant inlets, the temperature ($T_{c,i}$) and total pressure are set uniformly with a value of 339 K and 3.464 atm, respectively. To perform the highest effectiveness of film cooling as can be, the adiabatic wall is given at the outlet of the forward and aft coolant passages. This boundary condition is given at the top and bottom of the mainstream cascade as well. Two sides of the cascade are set as the periodic condition following the configuration of the annular cascade. For turbulence quantity, uniform turbulence intensity and length scale at the mainstream inlet are used and their values are 10 % and 0.4 cm, respectively. For the perfectly smooth surface case, K_s is set as 0.

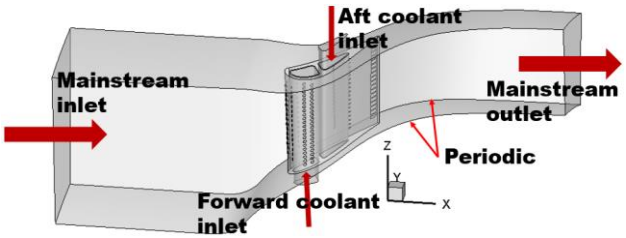

FIGURE 5: BOUNDARY CONDITIONS

According to the objective of the present study, the cooling performance sensitivity is predicted through three parameters which affect flow fields around the vane and heat transfer between the hot mainstream and the vane surface i.e. PR, $T_{c,i}$, and K_s. The variations of the three parameters are listed in Table 1.

TABLE 1: INDEPENDENT VARIABLES USED AS SENSITIVITY PARAMETERS

Parameter	Range of variation
Pressure ratio (PR)	1.67 - 2.70
Increment of coolant inlet temperature ($\Delta T_{c,i}$; %)	0 - 8
Surface roughness (K_s; μm)	0 - 80

For material property, the air is used for the mainstream and coolant and it is assumed as an ideal gas, whereas the vane structure is made of steel. All properties of the materials are given in Table 2, as previously studied by Zhang et al. [22] and Prapamonthon et al. [26].

TABLE 2: DETAILS OF MATERIAL PROPERTIES [22,26]

Property	Steel	Air
Density (kg/m^3)	8055	Ideal gas
Thermal conductivity (W/m·K)	11.2 + 0.0144T	0.01019 + 0.000058T
Specific heat capacity (J/kg·K)	438.5 + 0.177T	938 + 0.196T
Viscosity (kg/m·s)	-	Sutherland Law

*T in Kelvin

COOLING EFFECTIVENESS

To perform the cooling performance of the 1st stage nozzle guide vane, the cooling effectiveness denoted by ϕ is analyzed because it is linked directly to the vane temperature under the conductive wall condition. The cooling effectiveness is expressed mathematically as the equation (3).

$$\phi = \frac{T_\infty - T_w}{T_\infty - T_{c,in}} \quad (3)$$

The equation (3) is used to evaluate the surface cooling effectiveness. Furthermore, to perform the cooling performance sensitivity, the equation (3) is also used to compute the volume cooling effectiveness, and for this case, T_w is replaced with the volume vane temperature, T_{me}. It is expected that the cooling effectiveness is in a range of $0 < \phi < 1$ for real situations and all simulations of the present work. In addition, the heat transfer coefficient defined as the equation (4) is used to explain heat transfer phenomena at the vane surfaces also.

$$h = \frac{q_{flux}}{T_\infty - T_w} \quad (4)$$

where T_∞ is used as the temperature reference. The sign of the heat transfer coefficient corresponds to q_{flux}, namely, a positive value means that thermal energy transfers from the hot gas to the vane. But, if the thermal energy transfers oppositely, it shows a negative value.

NUMERICAL VALIDATION

To ensure that numerical results predicted by CFD/CHT approach are acceptable and reliable enough, the numerical result must be validated aerodynamically and thermally. In fact, the aerodynamic validation was done by Zhang et al. [22] by comparing the predicted Mach number distribution along the surface at midspan with the Mach number obtained by the experiment of Timko [25]. The Mach number predicted by SST k-ω model agreed well with that obtained by the experiment, as shown in Fig. 6. However, the thermal validation was not verified due to the lack of thermal experimental data from Timko [25] and other opened literature. Therefore, the present work needs to conduct the prediction of the cooling performance sensitivity under the assumption that the aerodynamics of fluid flow is of fundamental importance to heat transfer process accordance with the governing equations of fluid flow and heat transfer, including the equation of state for compressible flows. The method which demonstrates the ability to get a good aerodynamic agreement on the results of Mach number, pressure, and velocity distributions could result in a reasonable and acceptable thermal field, as seen in previously published papers [4-6, 12-14]. So far, the success in using SST k-ω to predict heat transfer in transonic cascades has been presented continuously, for instance, Ho et al. [27]. Therefore, the validation of aerodynamic results done by Zhang et al. [22] is still meaningful for the thermal prediction and the solver with SST k-w model is employed for the subsequent calculations of the present work.

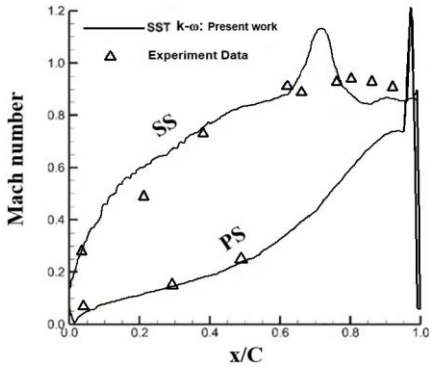

FIGURE 6: AERODYNAMIC VALIDATTION BY ZHANG ET AL. [22].

RESULTS AND DISCUSSION

Results for The Reference Case

Before discussing the effects of the pressure ratio, surface roughness and coolant inlet temperature on the cooling performance sensitivity, numerical results of the perfectly smooth vane are conducted under the basic boundary condition as the reference case. The surface cooling effectiveness and heat transfer coefficient distributions on the vane surface are presented. Fig. 7 shows contours of the cooling effectiveness and relatively high values of the cooling effectiveness are observed in the downstream of the exit of film holes. The highest cooling effectiveness is found in the downstream region close to the exit of fan-shaped film holes, R1 on the SS. These phenomena are

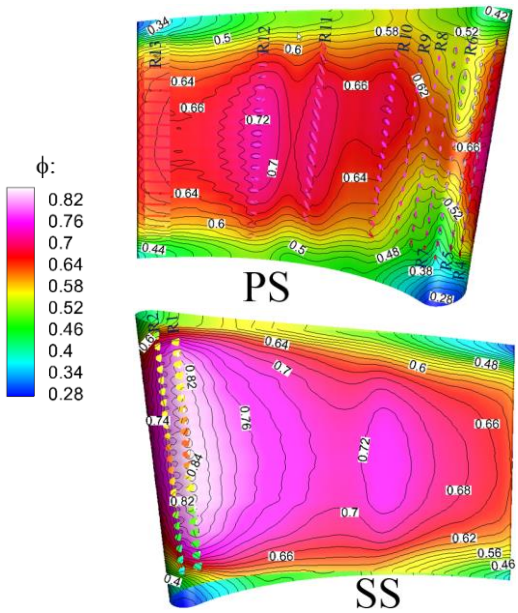

FIGURE 7: COOLING EFFECTIVENESS DISTRIBUTION ON VANE SURFACE FOR REFERENCE CASE

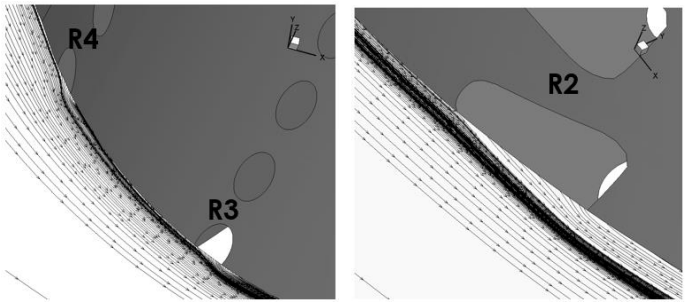

FIGURE 8: FLOW FIELD OF COOLING AIR/HOT GAS FOR REFERENCE CASE

reasonable because such regions are the location where cooling air just comes out of the film holes, as shown in Fig. 8. Therefore, effects of the cooling air become very strong, especially in the outlet regions of the rows R1 and R2 which can provide a relatively large amount of the cooling air due to a larger area of the fan-shaped exit. This can be confirmed from negative heat transfer coefficient and heat flux which is found in the downstream regions close to the exit of the film holes as shown in Figs. 9 and 10, respectively, Therefore, the wall temperatures in such regions are relatively low when comparing to other regions. However, because local static pressure in the LE and PS is relatively high and the film holes of the rows R5 - R9 are installed in the radial direction, so the cooling air emitted by these holes becomes lower effective for film protection. This leads to higher temperatures and lower cooling effectiveness on the vane surfaces which are close to the rows R5 - R9 when comparing to other regions. Similarly, this phenomenon can be also confirmed by the contours of heat transfer phenomena in Figs. 9 and 10. Fig. 7 also indicates regions where are scarcely

cooled by the cooling air and certainly these regions show lower cooling performance than the regions where are influenced by the film cooling. Another observation is that the cooling effectiveness ups again in the further downstream on the SS (the rear portion of the SS). This may be because that position consists of a lot of coolant passages of the slot holes of the row R13, including effects of flow transition. These result in lower heat flux driven by lower differences in the temperature between the cold-side and hot-side walls. As a result, the wall temperature decreases and the cooling effectiveness increases.

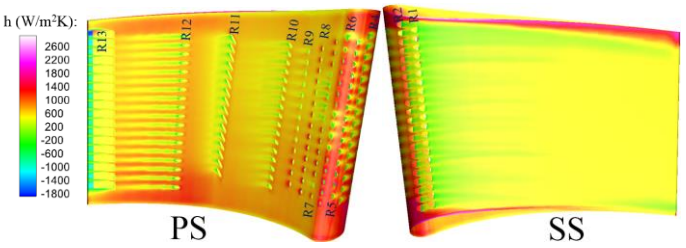

FIGURE 9: HEAT TRANSFER COEFFICIENT DISTRIBUTION ON VANE SURFACE FOR REFERENCE CASE

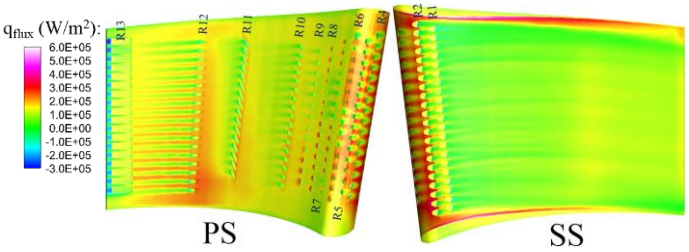

FIGURE 10: HEAT FLUX DISTRIBUTION ON VANE SURFACE FOR REFERENCE CASE

Next, the effects of the pressure ratio, surface roughness and coolant inlet temperature on the cooling performances are discussed in terms of the surface cooling effectiveness and heat transfer coefficient along the vane surface at midspan where is usually represented as the whole vane. It should be noted that for following graphs, "x/C = 0" indicates the stagnation position, "x/C > 0" means the position along the vane suction surface, and "x/C < 0" represents the position along the vane pressure surface.

Effects of Pressure Ratio

Fig. 11 presents the cooling effectiveness as PR ups from 1.67 to 2.7. It can be seen that PR increases the cooling effectiveness considerably in the rear portion on both PS (-1.0 < x/C < -0.7) and SS (0.5 < x/C < 1.0), but decreases the cooling effectiveness significantly in a range of -0.3 < x/C < 0.1 on the PS-LE-SS region. These phenomena are reasonable due to the fact that local static pressure at the exit of fan-shaped film holes of the rows R1 and R2 on the SS and axial film holes of the row R12 on the PS decreases with PR, as shown in Fig. 12. Therefore, cooling air emitted from such film holes may be more promoted by higher local momentum ratio, thereby improving the cooling effectiveness and its cooling performance in the rear portion of the PS and SS. Additionally, the high momentum of the cross-flow mainstream caused by increasing PR in the PS-LE-SS region may impede cooling air emitted from film holes in this region. This brings about low cooling effectiveness in such region and these phenomena can be found in the corresponding distribution of the heat transfer coefficient in Fig. 13 as well.

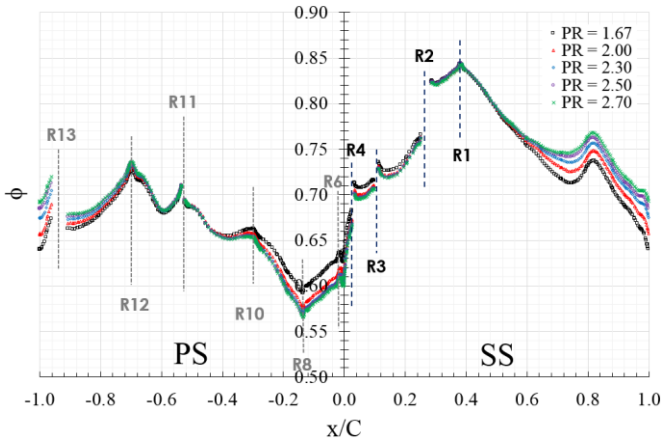

FIGURE 11: COOLING EFFECTIVENESS DISTRIBUTIONS AT MIDSPAN AT DIFFERENT PRESSURE RATIOS

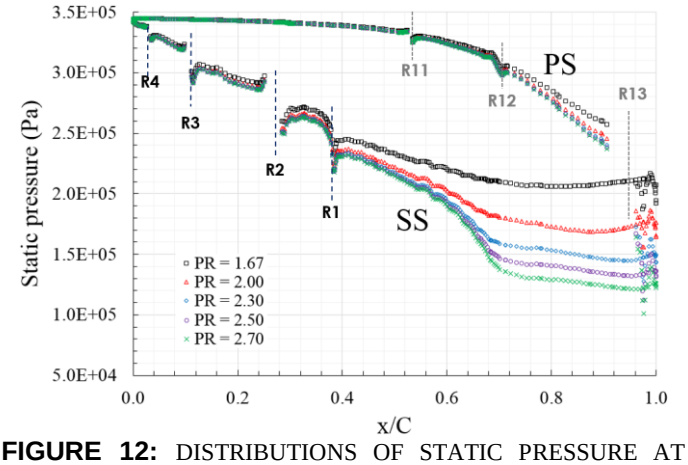

FIGURE 12: DISTRIBUTIONS OF STATIC PRESSURE AT MIDSPAN AT DIFFERENT PRESSURE RATIOS

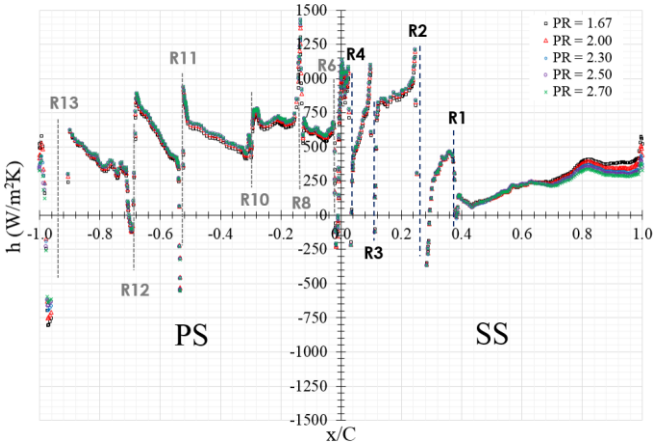

FIGURE 13: DISTRIBUTIONS OF COEFFICIENT OF HEAT TRANSFER AT MIDSPAN AT DIFFERENT PRESSURE RATIOS

Effects of Surface Roughness

Fig. 14 presents the distribution of the cooling effectiveness under the effects of the physical roughness height. Obviously, in general, the cooling effectiveness drops with the increment of K_s, especially in the further downstream regions of the film holes. This may be explained by the fact which is found in the distribution of heat transfer coefficients, as seen in Fig. 15.

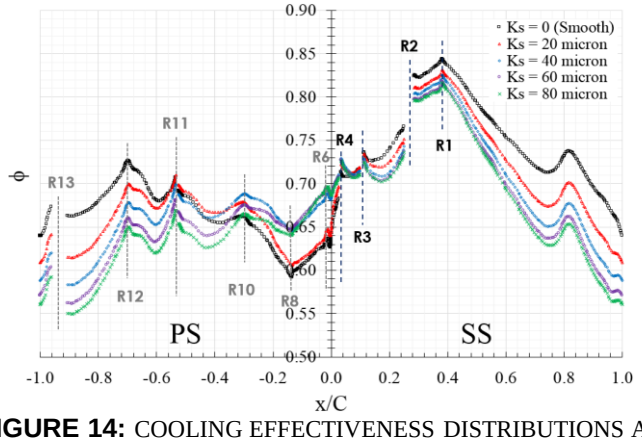

FIGURE 14: COOLING EFFECTIVENESS DISTRIBUTIONS AT MIDSPAN AT DIFFERENT SURFACE ROUGNESS HEIGHTS

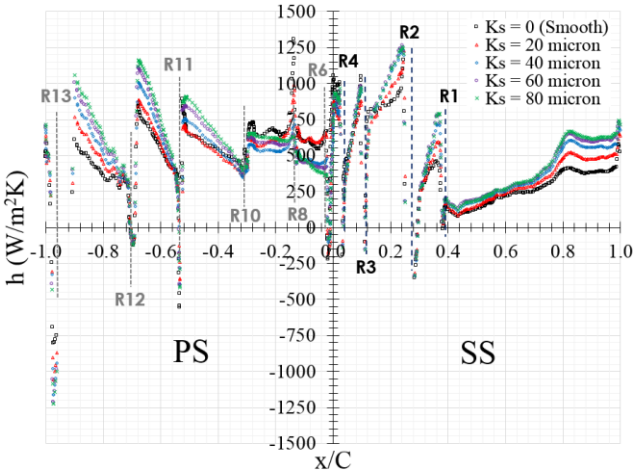

FIGURE 15: DISTRIBUTIONS OF COEFFICIENT OF HEAT TRANSFER AT MIDSPAN AT DIFFERENT SURFACE ROUGNESS HEIGHTS

The phenomenon shown in Fig. 15 indicates that the heat transfer coefficient rises drastically since K_s increases in the further downstream regions of the film holes. This is reasonable because according to the roughness model, the area of heat transfer increases with K_s. This phenomenon is lessened in the regions close to the exit of film holes due to more intense film protection. Nevertheless, uncertain variations of the cooling effectiveness are noticed in the PS-LE-SS region where is noted by the rows R3 – R10 in a range of $-0.3 < x/C < 0.1$. This may be explained by the fact that because such region in the PS is sensitive to turbulence quantities. The role of the surface roughness effects is important increasingly as K_s disturbs increasingly the viscous sublayer. Therefore, more complex flow instability is triggered off and the wall surface temperature is changed with uncertain heat transfer, as seen in Fig. 16 for example at the maximum roughness height, $K_s = 80$ μm.

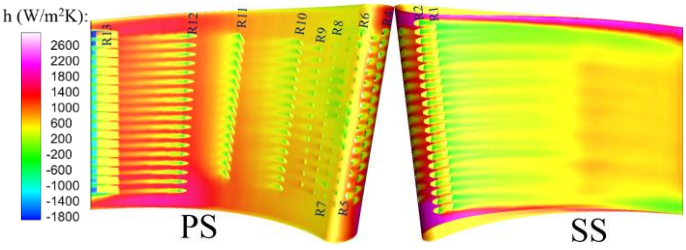

FIGURE 16: DISTRIBUTIONS OF COEFFICIENT OF HEAT TRANSFER AT $K_s = 80$ μm.

Effects of Coolant Inlet Temperature

Fig. 17 shows the distribution of the cooling effectiveness as the coolant inlet temperature rises from 0 to 8 %. Undoubtedly, the increase in the coolant inlet temperature reduces the cooling effectiveness uniformly. Therefore, the trend of the cooling effectiveness distributions obtained by increasing the coolant inlet temperature is the same as the reference case does, but completely different from that obtained by increasing K_s and PR. Realistically, the physical change in the surface roughness and the aerodynamic change in the pressure ratio involve the direct impact on the hot-side wall. These changes affect heat transfer between the hot gas and the vane surfaces directly. Although the increment in the coolant inlet temperature affects the temperature of the cooling air providing the film protection on the vane surface, it comes from the cold-side wall. Thus, this leads to totally different phenomena and Fig. 18 indicates the evidence of this difference. Namely, the heat transfer coefficients barely change with the coolant inlet temperature. It is reasonable due to the fact that the driving force between the hot-side and cold-side walls is reduced as the coolant inlet temperature rises directly. As a result, the amount of thermal load at the hot-side wall needs to decrease, as shown in Fig. 19 for example at the maximum increment in the coolant inlet temperature, $T_{c,in} = 8\%$.

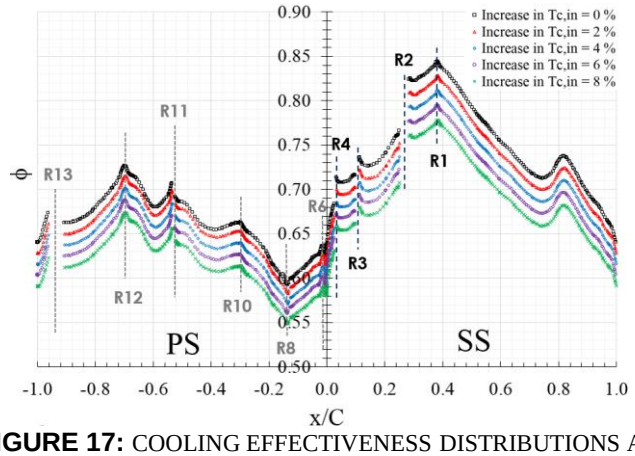

FIGURE 17: COOLING EFFECTIVENESS DISTRIBUTIONS AT MIDSPAN AT DIFFERENT INCREMENT OF COOLANT INLET TEMPERATURES

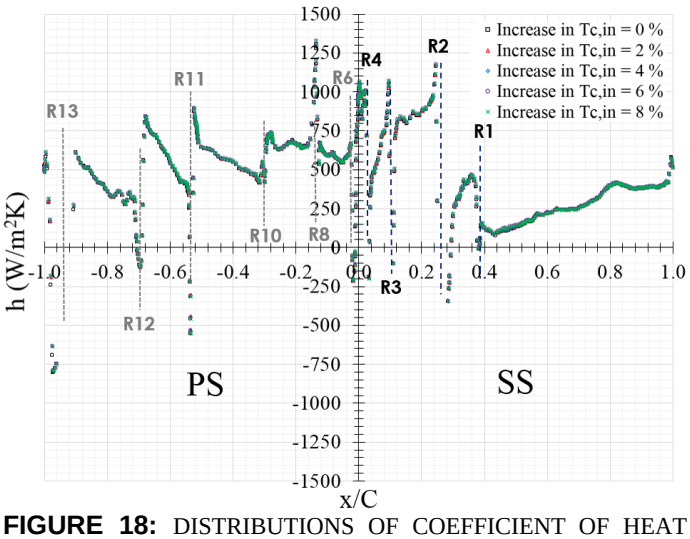

FIGURE 18: DISTRIBUTIONS OF COEFFICIENT OF HEAT TRANSFER AT MIDSPAN AT DIFFERENT INCREMENT OF COOLANT INLET TEMPERATURES

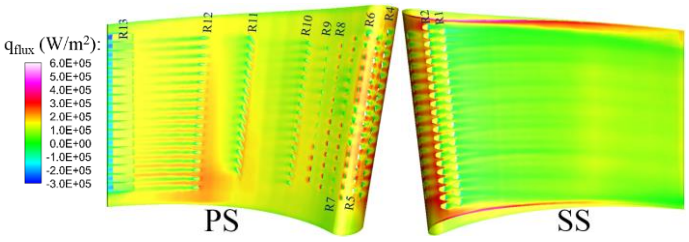

FIGURE 19: HEAT FLUX DISTRIBUTION ON VANE SURFACE WHEN COOLANT INLET TEMPERATURE INCREASES 8%

Lastly, further investigation into the cooling performance sensitivity under the effects of the pressure ratio, surface roughness, and coolant inlet temperature are discussed. Average (Ave.), maximum (Max.) and minimum (Min.) cooling effectiveness is simultaneously considered with corresponding temperature differences (ΔT). It should be noted that in this section the term "volume cooling effectiveness" is used.

Cooling Performance Sensitivity

Although the velocity of hot gas entering the part of moving blades of gas turbines depends upon the pressure ratio of the stationary vanes, this drop ratio in the mainstream passage has a directly unfavorable influence on the aerodynamic performance of the 1st stage of turbine vanes. Moreover, this influence brings about low cooling performance of the vane, as described previously. In order to obtain a better understanding of the variation of the cooling effectiveness, the cooling performance sensitivity under the effects of the pressure ratio is investigated in this part. Fig. 20 shows that T_{av} decreases linearly as the PR increases, in other words, ϕ_{av} is improved with the PR. However, this reduction is small, namely, only a 3.2 K reduction is reached though the PR ups to the maximum value of 2.7. Fig. 20 also indicates that T_{max} increases slightly with the PR, a 3 K rise at PR = 2.7. But, the increment in T_{max} tends to be alleviated, so ϕ_{min} is somewhat deteriorated when the PR rises. These phenomena may suggest the dominance of better cooling obtained in the rear portion of the vane PS and SS at higher PRs as explained previously, though the higher PRs have the strong adverse effects on cooling performance in the LE-downstream PS. Besides, it can be seen that T_{min} and ϕ_{max} vary trivially with the PR. This is reasonable and corresponding to the previous explanation that the PR has a direct impact on the hot-wall side due to the change in the aerodynamic condition, but an indirect influence on the thermal condition.

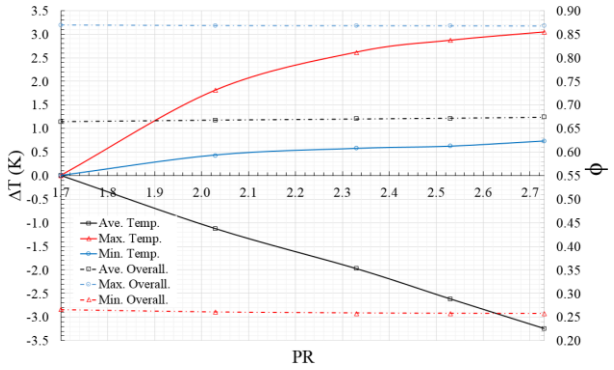

FIGURE 20: EFFECTS OF PRESSURE RATIO ON COOLING EFFECTIVENESS

In fact, the surface roughness is changed naturally due to deposition and corrosion after the turbine airfoils run for long hour services. Besides, in the manufacturing process of the turbine vane, the surface roughness is also an uncontrollable factor. In this section, the cooling performance sensitivity under varying the surface roughness is investigated as known that the roughness effect can change the aerothermal conditions of the turbine airfoils physically, and leads to the significant alteration of the flow field and heat transfer of the airfoils. As seen in Fig. 21, significant reductions in ϕ_{av} and ϕ_{min} are observed when K_s rises in the investigated range. The figure indicates that a rise in K_s of 80 μm results in 16 K and 17 K increments of T_{av} and T_{max}, thereby lowering ϕ_{av} and ϕ_{min}, respectively. However, the uncertain variation of T_{max} is also found in the range of $0 < K_s < 40$ μm, especially at $K_s = 20$ μm. This phenomenon may be explained by the fact that as T_{max} should be located in the hot-side wall which obtains the direct impact of the change in the surface roughness, and K_s^+ obtained from K_s in this range is in the zone of the transitional roughness. Thus, although the surface roughness effects become important increasingly, the effects are still unstable because of the instability of viscous sublayer disturbance caused by the increasing roughness. In addition, as well known that cooling effectiveness on the PS is quite sensitive to the turbulence of the mainstream. This also results in the variation of the cooling effectiveness with the roughness. Fig. 21 also indicates a decreasing trend of ϕ_{max} as K_s increases, and this reduction is lower than ϕ_{av} and ϕ_{min}. This seems unsurprising due to the fact that ϕ_{max} which is linked to T_{min} is in the cold-side wall, so the coolant effects become dominant and stronger than the effects caused by the roughness, as seen that a 6 K rise in T_{min} provided by the maximum roughness height only.

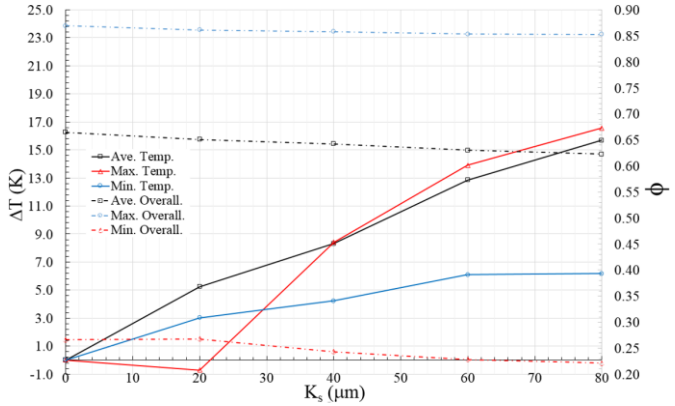

FIGURE 21: EFFECTS OF SURFACE ROUGNESS HEIGHT ON COOLING EFFECTIVENESS

To maintain the metal temperature of the vane below the maximum allowable temperature, the cooling air is taken from the compressor discharge and directed to the turbine vane to provide efficiently adequate cooling. When the coolant flows through supply passages till the exit of film holes, its temperature increases as its pressure reduces. Hence, the effects of the increase in the coolant inlet temperature supplied by the compressor on the cooling effectiveness sensitivity of the vane are investigated. Fig. 22 presents the variations of the vane cooling effectiveness and temperature with the increase in coolant inlet temperature. It is found that the vane cooling effectiveness and temperature vary linearly with the increase in the coolant inlet temperature. Obviously, Fig. 22 indicates that an 8 % rise in the coolant inlet temperature causes 18 K and 24 K increments in the T_{av} and T_{min}, respectively, thereby reducing ϕ_{av} and ϕ_{max} significantly. These phenomena are reasonable because ϕ_{max} is directly linked to T_{min}, which should exist in the cold-side wall. Therefore, when the coolant inlet temperature increases, T_{min} increases directly and results in the dramatic reduction of ϕ_{max}. Moreover, this dramatic reduction also leads to the significant reduction of ϕ_{av} because the variation of ϕ_{av} depends upon the variation of the vane metal temperature from the hot-side wall to the cold-side wall. This driving force is directly linked to the temperature difference between hot and cold sources. When the coolant inlet temperature increases, the driving force decreases. As a result, ϕ_{av} is reduced in the circumstances. Another observation is that the reduction of ϕ_{min} is lower than that of ϕ_{av} and ϕ_{max} in the investigated range, increasing 7 K in T_{max} from the 8% rise in the coolant inlet temperature. This may be explained by the fact that ϕ_{min} is related to T_{max} which exists in the hot-side wall, especially in regions where are cooled ineffectively by cooling air. The increment in the coolant inlet temperature affects T_{max} indirectly and the change in T_{max} is small. As seen previously in Fig. 18, the increase in the coolant inlet temperature has a small effect on the heat transfer coefficient. Consequently, the increase in T_{max} is lower than that in T_{av} and T_{min}.

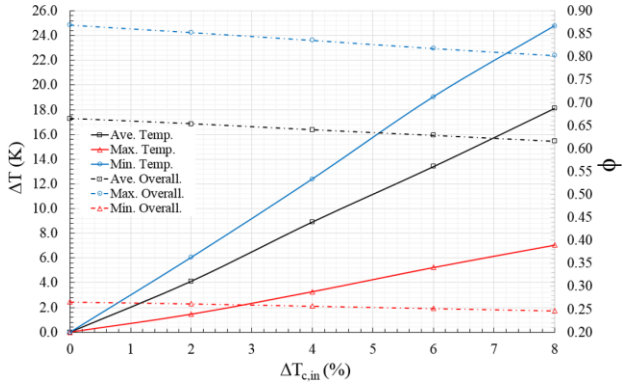

FIGURE 22: EFFECTS OF INCREASE IN COOLANT INLET TEMPERATURE ON COOLING EFFECTIVENESS

CONCLUSION

In this work, the CFD/CHT approach is used to numerically predict sensitivity of the cooling performances of a gas-turbine vane under aerodynamic and thermal conditions caused by three parameters i.e. pressure ratio, coolant inlet temperature and height of vane surface roughness. A simulated vane in this work is selected from one of 46 vanes of the 1st stage nozzle guide vanes of a high-pressure turbine reported by NASA Energy Efficient Engine program. The vane is film-cooled numerously and impinged by two baffles within coolant passages. Uncertainties of some parameters, which affect turbine vane heat transfer, are investigated. Numerical results show that the coolant inlet temperature and physical surface roughness have significant effects on the vane cooling performances. The 8% increase in the coolant inlet temperature results in 18 K increment in the vane average temperature. The 16 K and 17 rises in the vane average and maximum temperatures, respectively, are caused by the maximum roughness height i.e. 80 μm. Additionally, although the vane average temperature is reduced at higher pressure ratios, this effect is slight. Only 3.2 K reduction is obtained. It should be mentioned that since the numerical prediction of this work is validated aerodynamically only, heat transfer part is carried out under the favorable assumption of the governing equations of fluid flow and heat transfer, including the equation of state for compressible flows. Hence, the conclusion drawn here should be extended cautiously.

ACKNOWLEDGEMENTS

This paper is supported by National Key Research & Development Projects (Grant No.2017YFB0202802), National Natural Science Foundation of China (11702297), and the Strategic Priority Research Program of the Chinese Academy of Sciences (XDB22020101). The first author would like to thank the Chinese Academy of Sciences (CAS) for giving a very good opportunity to research at the Institute of Mechanics under the PIFI postdoctoral programme. In addition, the first author would like to thank Professor Jianhua Wang, Dr. Huazhao Xu, and Mr. Qingbo Zhang, University of Science and Technology of China, for their support and guidance. Finally, the special support of King Mongkut's Institute of Technology Ladkrabang is acknowledged as well.

REFERENCES

[1] Mazur, Z., Rossete, A.H., Illescas, R.G., and Ramírez, A.L., 2005. "Analysis of conjugate heat transfer of a gas turbine first stage nozzle," ASME Paper No. GT2005-68004.

[2] Kusterer, K., Hagedorn, T., Bohn, D., Sugimoto, T., and Tanaka, R., 2006, "Improvement of a film-cooled blade by application of the conjugate calculation technique," J. Turbomach., Vol. 128, pp. 572-578.

[3] Silieti, M., Kassab, A.J., and Divo, E., 2009, "Film cooling effectiveness: comparison of adiabatic and conjugate heat transfer CFD models," Int. J. Therm. Sci., Vol. 48, pp. 2237–2248.

[4] Mangani, L., Cerutti, M., Maritano, M., and Spel, M., 2010, "Conjugate heat transfer analysis of NASA C3X film cooled vane with an object-oriented CFD code," ASME Paper No. GT2010-23458.

[5] Yoshiara, T., Sasaki, D., and Nakahashi, K., 2011, "Conjugate heat transfer simulation of cooled turbine blades using unstructured-mesh CFD solver," AIAA Paper No. AIAA 2011-498.

[6] Ke, Z.Q., and Wang, J.H., 2016, "Conjugate heat transfer simulations of pulsed film cooling on an entire turbine vane," Appl. Therm. Eng., Vol. 109, pp. 600–609.

[7] Ni, R.H., Humber, W., Fan, G., Johnson, P. D., Downs, J., Clark, J.P., and Koch, J.P., 2011, "Conjugate heat transfer analysis of a film-cooled turbine vane," ASME Paper No. GT2011-45920.

[8] Bohn, D. E., and Tummers, C., 2003, "Numerical 3-D conjugate flow and heat transfer investigation of a transonic convection-cooled thermal barrier coated turbine guide vane with reduced cooling fluid mass flow," ASME Paper No. GT2003-38431.

[9] Ba, W., Liu, L.G., and Liu, H., 2018, "Aero-thermal coupled predictive model for preliminary gas turbine blade cooling analysis," ASME Paper No. GT2018-75089.

[10] Zecchi, S., Arcangeli, L., Facchini, B., and Coutandin, D., 2004, "Features of a cooling system simulation tool used in industrial preliminary design stage," ASME Paper No. GT2004-53547.

[11] York, W.D. and Leylek, J.H., 2003, "Three-dimensional conjugate heat transfer simulation of an internally-cooled gas turbine vane", ASME Paper No. GT2003-38551.

[12] Alizadeh, M., Izadi, A., and Fathi, A., 2014, "Sensitivity analysis on turbine blade temperature distribution using conjugate heat transfer simulation," J. Turbomach., Vol. 136, pp. 011001.

[13] Alizadeh, M., Izadi, A., Fathi, A., and Khaledi, H., 2012, "Flow and heat transfer analysis of turbine blade cooling passages using network method," ASME Paper No. GTINDIA2012-9644.

[14] Reyhani, M.R., Alizadeh, M., Alireza Fathi, A., and Khaledi, H., 2013, "Turbine blade temperature calculation and life estimation - a sensitivity analysis," Propul. Power Res., Vol. 2(2), pp. 148-161.

[15] Haubert, R. C., Hsia Sr., E., Maclin, H. M., Noe, M. E., and Brooks, R. O., 1980, "High pressure turbine blade life sensitivity," AIAA Paper No. 80-1112.

[16] Kim, B.S., Kim, B.S., Choi, W.S., Musgrove, G.O., McFarland, J., Fierro, F., and Ransom, D.L., 2012, "Gas turbine blade stress and temperature sensitivity to turbine inlet profile and cooling flow," ASME Paper No. GT2012-69603.

[17] Roos, T., 2005, "NGV Trailing edge ejection slot size sensitivity study," Paper No. ISABE-2005-1158.

[18] Williams, R.P., Dyson, T.E., Bogard, D.G., and Bradshaw, S.D., 2014, "Sensitivity of the overall effectiveness to film cooling and internal cooling on a turbine vane suction side," J. Turbomach., Vol. 136, pp. 031006.

[19] Nadali, H.N., Karlsson, M., Kinell, M., and Utriainen, E., 2012. "CFD based sensitivity analysis of influencing flow parameters for cylindrical and shaped holes in a gas turbine vane," ASME Paper No. GT2012-69023.

[20] Espinosa, F., Portugal, A., Narzary, D., Cadena, F., Han, J., Kubiak, J., Blake, S., and Lara, H., 2008, "Influence of cooling flow rate variation on gas turbine blade temperature distributions," ASME Paper No. GT2008-50103

[21] Halila, E.E., Lenahan, D.T., and Thomas, T.T., 1982, "Energy efficient engine high pressure turbine test hardware detailed design report," NASA CR-167955, NASA Lewis Research Center.

[22] Zhang Q.B., Xu, H.Z., Wang, J.H., Li, G., Wang, L., Wu, X.Y., and Ma, S.Y., 2015, "Evaluation of CFD predictions using different turbulence models on a film cooled guide vane under experimental conditions," ASME Paper No. GT2015-42563.

[23] Nikuradse, J., 1933, "Laws for flows in rough pipes," VDI-Forchungsheft Series B, Vol. 4 (English translation NACA TM 1292, 1950).

[24] Cebeci, C., and Bradshaw, P., 1977, "Momentum transfer in boundary layers," Hemisphere Publishing Corporation, New York.

[25] Timko, L.P., 1984, "Energy efficient engine high pressure turbine component test performance report," NASA CR-168289, NASA Lewis Research Center.

[26] Prapamonthon, P., Xu, H.Z., Yang, W.S., and Wang, J.H., 2017, "Numerical study of the effects of thermal barrier coating and turbulence intensity on cooling performances of a nozzle guide vane," Energies, Vol. 10, pp. 362.

[27] Ho, K.S., Liu, J.S., Elliott, T., and Aguilar, B., 2016, "Conjugate heat transfer analysis for gas turbine film-cooled blade," ASME Paper No. GT2016-56688.